



Microstructured Radiators

Final Report

Authors: Philippe Ben-Abdallah

Affiliation: Nantes University-Laboratoire de Thermocinétique-France

ESA Researcher(s): Luzi Bergamin

Date: 01.07.2007

Contacts:

Philippe Ben-Abdallah

Tel: +33 (0) 2 40 68 31 17

Fax: +33 (0) 2 40 68 31 41

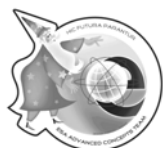
e-mail: pba@univ-nantes.fr

Leopold Summerer

Tel: +31(0)715655174

Fax: +31(0)715658018

e-mail: act@esa.int



Available on the ACT website
<http://www.esa.int/act>

Ariadna ID: 06/9501a
Study Duration: 2 months
Contract Number: 20270/06/NL/HE

I-Project Background and Motivation

Controlling the spatial or temporal coherence of thermal light a hot body emits when it relaxes to lower states is undoubtedly one of major objectives for improving the efficiency of numerous actual technologies such as thermophotovoltaic conversion devices, radiative cooling systems, infrared gas sensors and highly directional/narrow band thermal radiators. Until recently thermal sources were considered as objects that were able to emit light only over a broad band of the infrared spectrum. Today we know this paradigm is wrong¹⁻² and several partially coherent thermal sources have been already fabricated³⁻⁵. The physical origin of these unusual behaviors comes from the structures at the wavelength scale of materials used to fabricate these sources. Roughly speaking, in the first generation of partially coherent thermal sources, polar materials surmounted by an appropriate surface grating are used to diffract the surface phonon-polaritons into the far field. This principle has opened new prospects for radically changing the way light moves through them and has enabled to engineer the radiative properties⁶ of these media. However these effects are based on optical mechanisms which strongly limit their applications in the field of thermal emission. Indeed, for 1D grating, no lobe of emission can be observed in s-polarization since, in this case, no surface wave exists. Then, energy radiated by the source is localized in well defined directions only for p-polarization, the emissivity remaining globally isotropic for s-polarization.

One of the best achievements in the design of coherent thermal sources has been obtained later with photonic crystals⁶. These periodic dielectric structures-also known as photonic band gap (PBG) materials-have, for almost two decades, attracted much attention because of their high potentiality in numerous applied and theoretical fields (see Benisty et al. in Ref. [6]). At sufficient refractive index contrast, PBG forbid photons to propagate through them at certain frequencies, irrespective of propagation direction in space and polarization. Coupled with frequency selective surfaces photonic crystals have recently allowed the construction of narrow bands IR emitters⁷. These last years promising results have opened prospects for the fabrication of temporally coherent IR sources when a defect is introduced into a photonic crystal⁸⁻⁹. Such defects act like waveguides with a confinement achieved by means of the photonic band gap and not by total internal reflection as in traditional wave guides. The latest generation¹⁰ of partially coherent thermal sources, has been engineered by coupling polar layers with photonic crystals. These structures exhibit highly directional and narrow bands emission patterns for both p- and s-polarization states of the thermal light. Similar antenna-like emission patterns also have been achieved with completely different physical mechanisms using simple thin films¹¹ and more recently resonant cavities coupled with metallic layers¹².

Another direction of research has been recently explored for designing thermal antennae with left-handed material¹³ (LHM) which are engineered from one-dimensional periodic metallic structures.

Near the plasmon resonance of these structures, the effective optical index is close to zero. Therefore, in accordance with the Snell-Descartes laws, the radiation emitted by a source (a dipole) embedded in this medium is expected to be refracted around the normal to the surface. However, similarly to polar materials surmounted by surface gratings the strong spatial coherence (high directivity) observed with these structures is limited to transversal magnetic (TM) waves. Moreover, although these structures make it possible to consider many applications at localized frequencies they seem, because of the dispersion, much more difficult to exploit for designing spatially coherent thermal sources over a broad spectral band.

So far, all distinct approaches mentioned above have led to highly directional, narrow band partially coherent thermal sources. However it is not known whether the corresponding structures truly achieve the maximum permissible coherence degree. It is precisely the purpose of this research project to answer this question.

Study objectives

The ability to artificially grow, from modern deposition techniques, complex structural configurations of planar heterogeneous metallic/dielectric materials raises the issue of the best achievable thermal emitter that is with the highest directivity and/or with the narrowest band of emission in a given spectral range. This engineering design problem is formally a type of mathematical inverse problem. The research goal of the present program is precisely the achievement of a program to solve this problem. In this work we will develop, as a search algorithm of the optimal structure, a genetic algorithm (GA is a stochastic global optimisation method based on the natural selection process) dedicated to this task. We can expect in this way to design the ‘ultimate’ one dimensional thermal emitter with a spatial/spectral degree of coherence close to the limit imposed by the optical analogous of Heisenberg’s uncertainty principle¹⁴.

Description of intended research work

The project divides into three distinct areas of activity which follow a logical progression.

- a) Development of an inverse design software based on a genetic algorithm.
- b) Analysis of modes coupling in the optimal structures using FDTD simulations.
- c) Sensitivity of emission angles and emission frequency to temperature changes.

Results expected

-Development of an inverse design program software for one-dimensional heterogeneous structures.

- Design of “coherent” one-dimensional planar thermal sources.
- Understanding of optical mechanisms involved (modes coupling and mechanisms of emission enhancement).
- Studying the temperature dependence of emission spectra

II-Details on Project Activities

II-1 Development of an inverse design software based on a genetic algorithm.

The structures investigated in this project are shown in Fig. 1. They are one-dimensional stacks built by superposing nanolayers of different dielectric materials. All these composite materials are formed from M unit nanolayers of the same total thickness L . Each layer is either an emitting (lossy) or a nonemitting (transparent) material in the region of the infrared spectrum under investigation. The total number of all possible configurations that theoretically can be fabricated with N distinct materials is N^M . For binary structures made with 100 unit layers there are more than 10^{30} possible configurations. It will be as large as 10^{47} for three basis materials. Such a large space offers immense possibilities to sculpt the radiative properties of nanolayered composites. But, to explore effectively this vast space of composite materials and identify the structures which possess the desired properties, a rational searching method is needed. To do that we use a genetic algorithm¹⁵ (GA) which is a stochastic global optimisation method based on natural selection rules in a similar way to the Darwin’s theory of evolution. The main steps of GA are summarized hereafter. *Step 1*- The evolution process is started by generating an initial generation also called population (typically few tens to one thousand) of random structures. In parallel, we define some target radiative properties (for instance the spectral and directional emissivity $\varepsilon_{target}(\lambda, \theta)$ and reflectivity $r_{target}(\lambda, \theta)$) that we want to recover. Then, in order to select the best morphologies in this population, in comparison with these objectives functions, we calculate the radiative properties (transmittivity $t(\lambda, \theta)$, reflectivity $r(\lambda, \theta)$ and emissivity $\varepsilon(\lambda, \theta)$) of each individual by using their transfer matrix (see appendix). *Step 2*- The discrepancy between these targets and the radiative properties of current structures is measured by a fitness function under the form

$$J = \sum_P \int_{\theta_1}^{\theta_2} \int_{\lambda_{\min}}^{\lambda_{\max}} [\varepsilon_{target}(\lambda, \theta) - \varepsilon_{calc}^P(\lambda, \theta)]^2 d\theta d\lambda + \sum_P \int_{\theta_1}^{\theta_2} \int_{\lambda_{\min}}^{\lambda_{\max}} [r_{target}(\lambda, \theta) - r_{calc}^P(\lambda, \theta)]^2 d\theta d\lambda, \quad (1)$$

where the discrete sum operates over both states of polarization of the thermal light. *Step 3*- Once the fitness has been calculated, some population’s members are selected on the basis of their fitness function to become parents and to produce children structures in a breeding procedure known as

crossover (Fig.1). One of most natural selection rule is to keep only for the next generations the structures with a fitness function below a threshold.

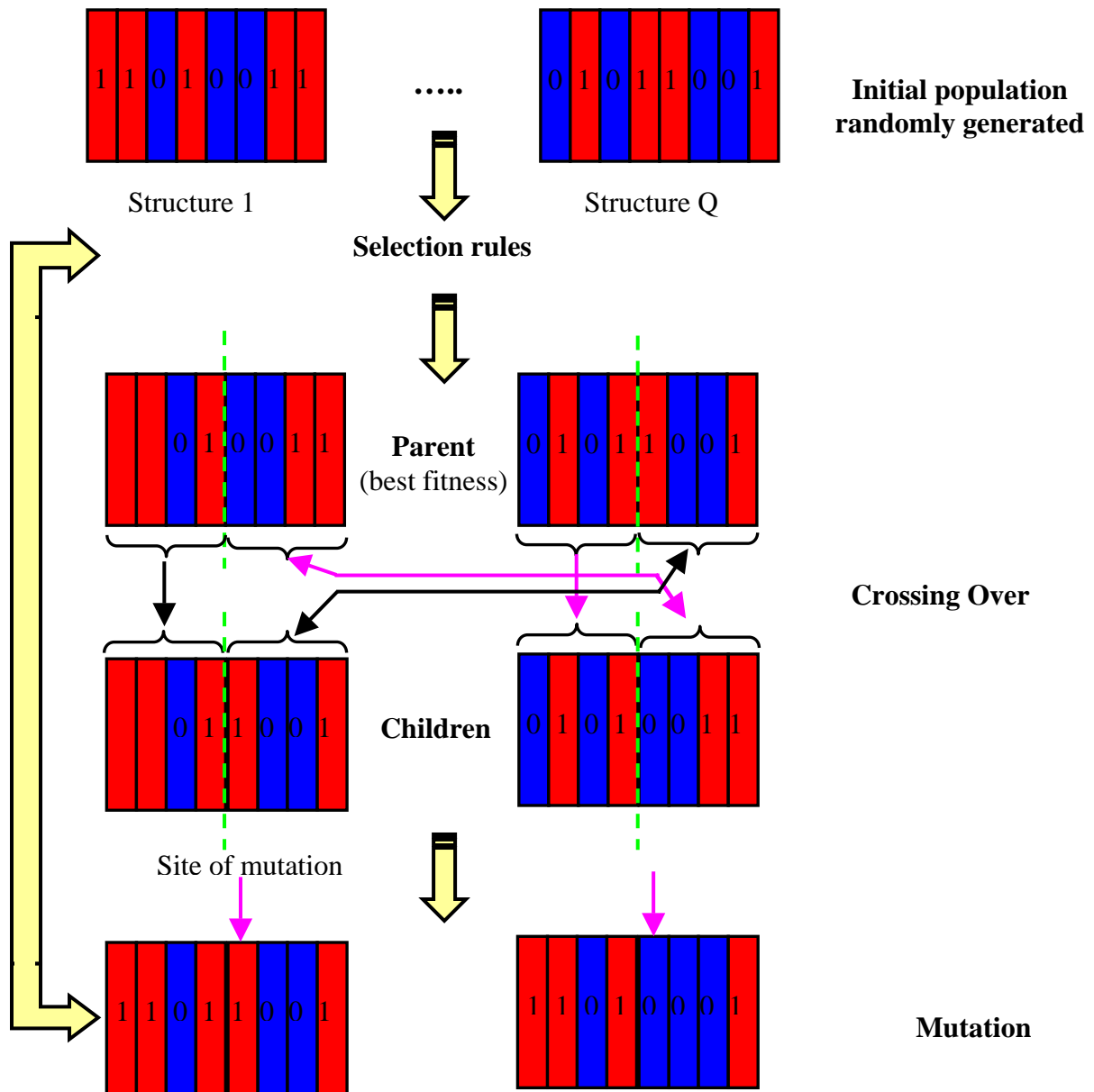


Fig.1. Principle of genetic algorithm (GA) used to design a binary nanostructured one-dimensional functional material. Here are described the main steps of GA : Initialization of a random population, selection of parents generation, cross over and mutation.

The crossover involves the creation of two children structures which are a combination of structural features of their parents. For example, by applying a simple one point crossover technique for binary structures, the parents 110010011 and **01011001** are split and recombined to form two children structures 11001**1001** and **0101**0011. *Step 4-* Some mutations are involved in the children's generation to improve the performances of the algorithm and avoid converging toward local minima. To do that we generate a random variable p_m which defined the probability for an arbitrary cell in a

structure at the m th generation to be changed. This step is fundamental to maintain a certain diversity in the children generation. When p_m is large, the evolution algorithm tends to search randomly over the discrete space of all possible structures and the population members remain far from the best structure. In contrary, when p_m is small the searching algorithm tends to the nearest local extremum. Thus, an appropriate choice of p_m is crucial for balancing the local convergence and the global search. To keep this mutation efficient we furthermore adjust p_m each I generations according to the following incrementing rule

$$\Delta p_m = \begin{cases} +\xi, & \gamma < 1/3 \\ 0, & 1/3 < \gamma < 2/3 \\ -\xi, & \gamma > 2/3 \end{cases}, \quad (2)$$

where ξ denotes the change of mutation probability and γ is the ratio of the averaged fit over the current population to the minimal fit. Then, we introduce some new structures randomly designed to keep the same total number of structures in every population. This operation introduces diversity throughout the evolution process. Finally we select new parent structures among this children population and go back to the selection step and so on until an optimal structure is found.

II-2 Design of “coherent” one-dimensional planar thermal sources (design examples).

We present here two nanostructured thermal sources that we have designed following the rational approach described above.

a-A quasi-isotropic source at ambient temperature

The first inverse designed source is a quasi-isotropic source that has been imagined to radiate in a narrow spectral band (Fig.2). To synthesis this quasi-monochromatic source we adopt a ternary structure consisting of silicium carbide (SiC), germanium (Ge) and telluride cadmium (CdTe) layers. This source is designed to operate in the range of wavelength $[8 \mu m; 14.5 \mu m]$. In this region both Ge and CdTe are transparent materials and their dielectric permittivities can be approximated¹⁶ by the constant values $\epsilon_{Ge} = 16$ and $\epsilon_{CdTe} = 7.29$. As for the SiC, it is the only dissipative material and its dielectric function is correctly described by the simple oscillating Lorentz model

$$\epsilon_{SiC} = \epsilon_{\infty} \left[1 + \frac{\omega_L^2 - \omega_T^2}{\omega_T^2 - \omega^2 - i\Gamma\omega} \right], \quad \text{where } \omega_L = 18.253 \times 10^{13} \text{ rad.s}^{-1}, \quad \omega_T = 14.937 \times 10^{13} \text{ rad.s}^{-1},$$

$\Gamma = 8.966 \times 10^{11} \text{ rad.s}^{-1}$ and $\epsilon_{\infty} = 6.7$ denote the longitudinal and transversal optical phonon pulsation, the damping factor and the high frequency dielectric constant, respectively. Moreover, all materials involved here are nonmagnetic in this wavelength range. As target emissivity we choose the

Gaussian function $\varepsilon_{target} = \varepsilon_{max} \exp[-Q^2 \ln \frac{16}{\varepsilon_{max}^4} (\lambda - \lambda^*)^2 / \lambda^{*2}]$ which is centred at

$\lambda^* = 12.6 \mu m$, the wavelength of upper edge of the phonons absorption band in SiC. At this wavelength, the SiC layers support evanescent modes regardless of the angle of incidence so that when these localized waves are excited from an external perturbation, the incident energy is resonantly transferred to SiC phonons and cause a large absorption of light. In accordance with the Kirchoff's law²⁰ this photon-photon coupling supports a strong emission at the same wavelength. Also, in order to use the structure as coating material we set a target reflectivity under the form $r_{target} = 1 - t_{target} - \varepsilon_{target}$ where $t_{target} \ll 1$ which allows only the thermal light close to λ^* to be transferred to the multilayered source from an eventual substrate, all the rest light being reflected back. The degree of spectral coherence of this source, measured by its quality factor $Q = \lambda^* / \Delta\lambda$ namely the ratio of the resonance wavelength over the full width at half maximum of the resonance, is set to 80 while the maximum of emissivity searched is $\varepsilon_{max} = 0.95$. For the present structure we use the following geometric parameters: $M=50$ and $d = L/M = 100 nm$. As for the fitness, it is minimized over the spectral range $[\lambda_{min} = 12.2 \mu m; \lambda_{max} = 12.8 \mu m]$ and the angular domain $[\theta_1 = 0; \theta_2 = 80^\circ]$. Figure 2 shows the designed structure obtained after $m=3100$ generations. One can see that the structure produced by ab initio design is highly disordered and very difficult to intuit a priori. Its reflectivity pattern plotted over the enlarged spectral range $[8 \mu m; 14.5 \mu m]$ shows the presence, out of λ^* , of a large and quasi complete (omnidirectional) band gap (excepted at oblique incidences) in the spectral range $[11 \mu m; 14 \mu m]$. So far, such omnidirectional band gaps had been observed only in periodic and quasi-periodic materials like photonic crystals¹⁷ and quasicrystals¹⁸⁻²⁰. This band gap is clearly desirable in the perspective of using this nanostructure as coating material. As for the emission spectrum, it is quasi-resonant ($\varepsilon \approx \varepsilon_{max}$) precisely at λ^* in this band gap for almost every directions of space.

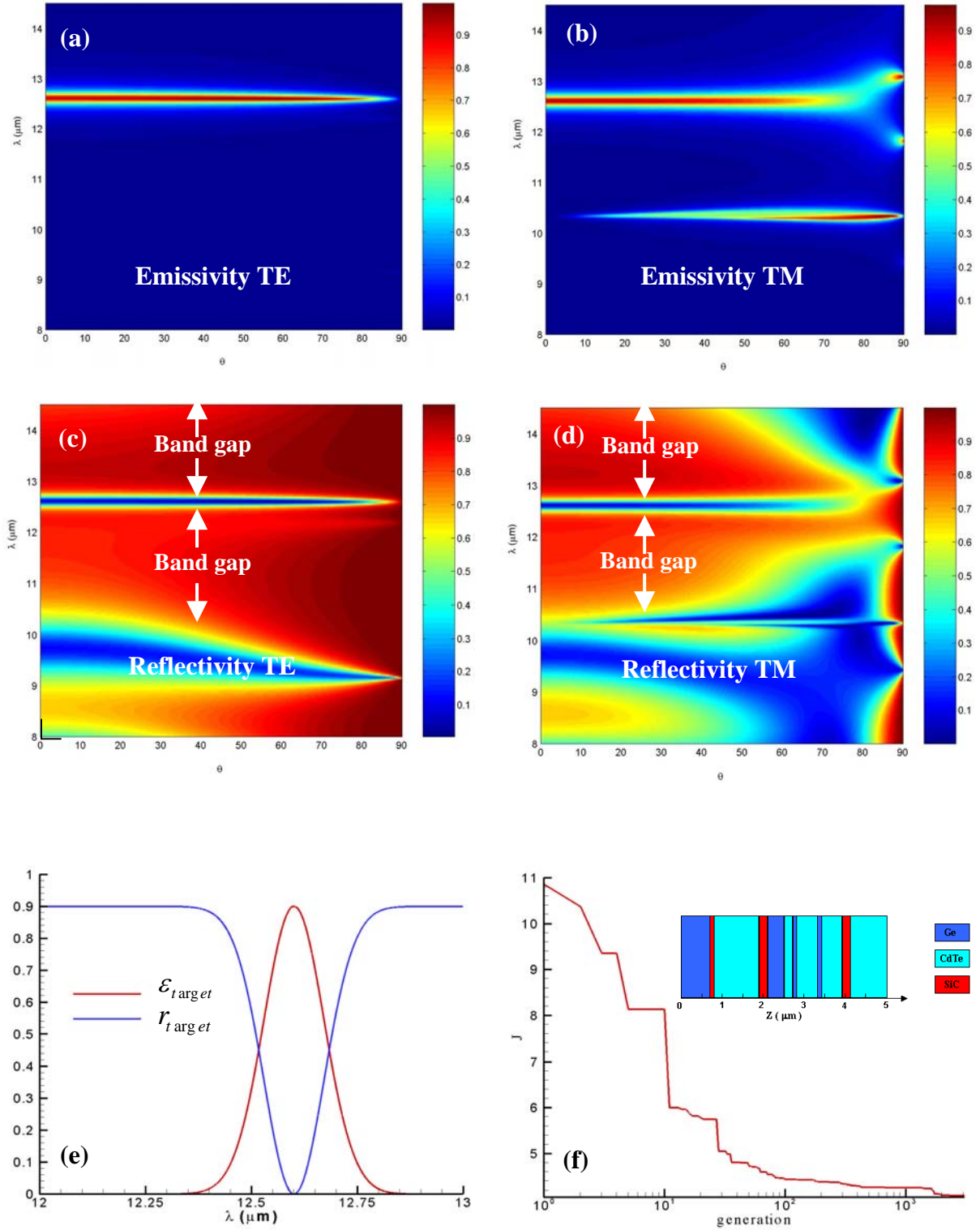


Fig.2. Spectral and directional emissivity (a-b) and reflectivity (c-d) of a quasi-monochromatic thermal source made with 50 nanolayers of SiC, Ge and CdTe 100 nm thick and designed by GA. The peak of emission which appears at $\lambda = 10.4\mu\text{m}$ in polarization TM at oblique incidence is outside of minimization domain (e) Target radiative properties. (f) Fitness function ($\times 0.001$) versus the generation number and structure of the designed source. GA parameters : $\lambda_{\min} = 12.2\mu\text{m}$, $\lambda_{\max} = 12.8\mu\text{m}$, $\theta_{\min} = 0^\circ$, $\theta_{\max} = 80^\circ$, $m = 3100$ and $I = 10$.

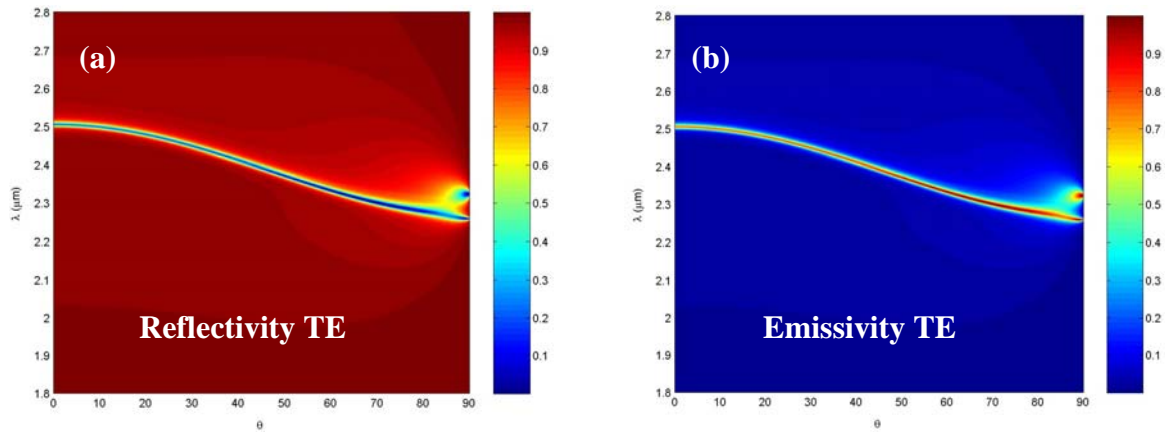
Hence the designed structure can be interpreted as a phonon-polariton resonant guide. Indeed, it behaves like a mirror in the band gap and converts any photon into atomic vibration (phonons) at λ^* by resonant photon-phonon coupling.

b-A partially coherent source in the near infrared

The second structure we have inverse designed is a multilayered plasmonic structure made with silver (Ag), silicon (Si) and glass (SiO₂) layers. Contrary to the first source, our goal here is to control the thermal emission not only in frequency but also in direction. The target emissivity and reflectivity plotted in Fig. 3 are defined in the spectral range [$\lambda_{\min} = 1.8 \mu\text{m}$; $\lambda_{\max} = 2.8 \mu\text{m}$] where Ag supports surface waves also called surface plasmon (SP). These waves are due to collective motion of electrons in Ag. In this spectral range the dielectric permittivities of Si and SiO₂ are well approximated¹⁹ by the real values $\epsilon_{\text{Si}} = 11.15$ and $\epsilon_{\text{SiO}_2} = 2.1025$ while the Ag permittivity is complex valued and

described by the free-electron/Drude model $\epsilon_{\text{Ag}} = 1 - \frac{\omega_p^2}{\omega(\omega - i\omega_c)}$, where

$\omega_p = 13.69 \times 10^{15} \text{ rad.s}^{-1}$ is the plasma pulsation and $\omega_c = 2.73 \times 10^{13} \text{ rad.s}^{-1}$ is the electron collision frequency. The geometric parameters of the studied structure have been set to $M=50$, and $d=50 \text{ nm}$. Figure 3 shows that the targets are relatively well recovered for both polarization states (only TE polarization is plotted) with an evolution process of 200 generations only. Once again the structure is highly disordered. As for the quality factor, it reaches approximately 238 at normal incidence and falls to about 200 at 60°. These values are the highest values reported so far with planar multilayer structures using Ag films.



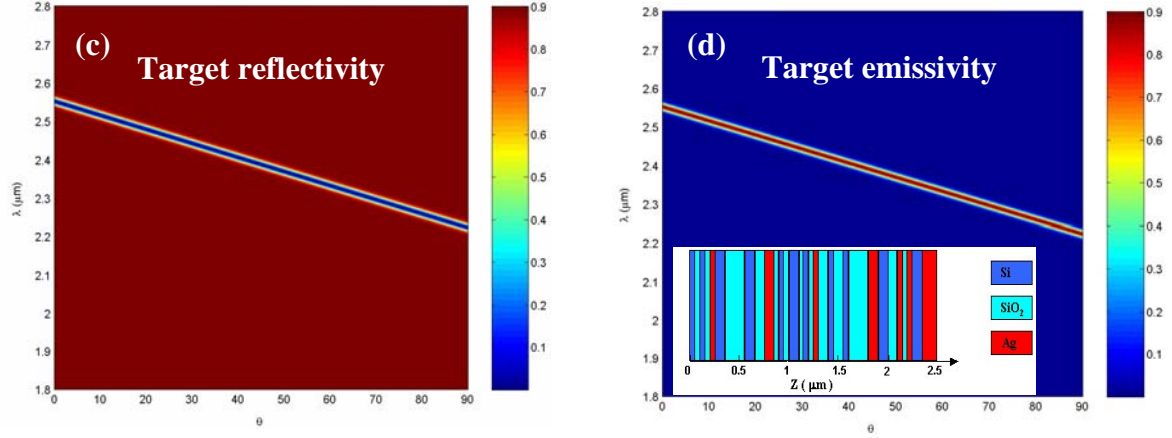


Fig.3. Spectral and directional reflectivity (a) and emissivity (b) in polarization TE of a partially coherent thermal source made with 50 nanolayers of Ag, Si and SiO₂ layers 50 nm thick and designed by GA. (c-d) Target radiative properties and structure of the designed source (insert of d). GA parameters : $\lambda_{\min} = 1.8\mu m$, $\lambda_{\max} = 2.8\mu m$, $\theta_{\min} = 0^\circ$, $\theta_{\max} = 90^\circ$, $m = 200$ (generations number) and $I = 10$.

II.3 Understanding of optical mechanisms involved

In order to find the physical origin of the partially coherent emission we now examine the field inside the designed structure when it is submitted to external (normalized) excitations. The result displayed in Fig. 4 shows that the intensity of the electric field inside the structure becomes locally much larger than 1 at the incidence angles and wavelengths where the emissivity pattern is maximum. As we can see on Fig.3, this is due to internal resonant mechanisms. Indeed, if we pay attention on the case where an incident wave of wavelength $\lambda = 2.4\mu m$ impinges the structure under an angle of 42° , we observe that the field at the interface between the Ag and SiO₂ layers at $z = 0.75\mu m$ is strongly enhanced by more than two orders of magnitude. Such a resonance, exponentially localized on both sides of the Ag layer, reveals the presence of a SP and demonstrates that the incident wave is able to couple with it. Thus, the energy of this propagative wave is resonantly transferred to SPs. Therefore, this coupling directly contributes to the strong emission of the structure in the angular lobe centred at 42° . In contrary, for all others angles of incidence at the same frequency and for all angles outside of the range $[2.25\mu m; 2.55\mu m]$ there is no significant enhancement of field in the structure and very few energy is absorbed by the Ag layers. Then, according to the Kirchoff's law, the thermal emission of the structure is very small.

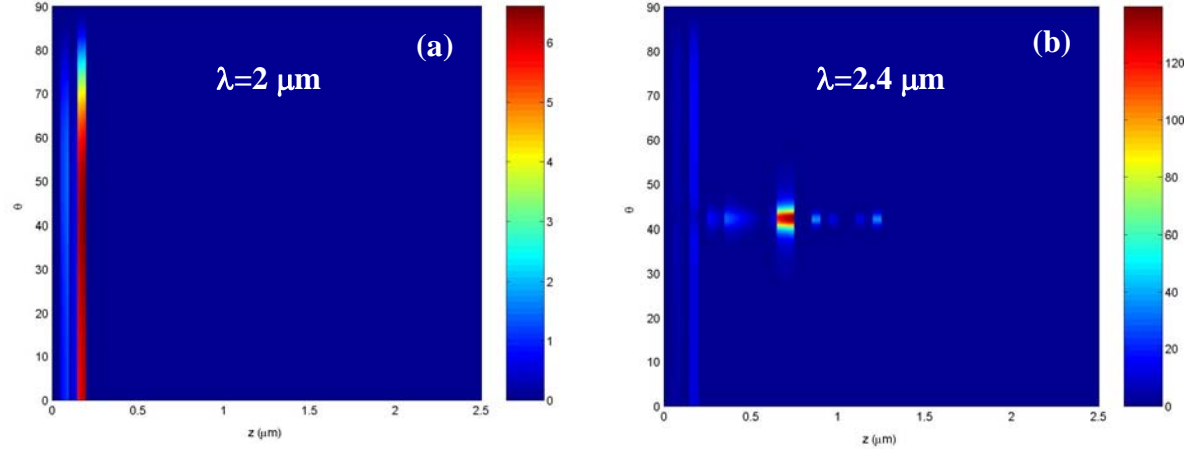


Fig.4. Modulus of the electric field (polarization TE) inside the inverse designed metallodielectric structure (cf. Fig. 3) when it is highlighted by an incoming field of unit magnitude. Wavelengths of excitation are $\lambda = 2\mu m$ (a) and $\lambda = 2.4\mu m$ (b). In (b), the strong intensity of field at $z = 750nm$ around 42° demonstrates the presence of a resonant coupling between the incident (propagative) wave and the surface (evanescent) waves supported by the metallic layer at this position. This resonance coincides with the emission peak observed in Fig.3 at 42° for $\lambda = 2.4\mu m$. Also a weak coupling between the surface plasmons and the incident wave is observed in (a) and (b) at $z = 200nm$. However, the comparison between Figs. 3 and 4 shows that the transfer of energy from photons to electrons in this region is too small to significantly participate to the thermal emission of the structure.

II.4 Temperature dependence of emission spectra

The analysis of previous sections did not take into account the temperature dependence of optical properties of dielectrics, semiconductors, and metals used to fabricate the radiators. Here we present the temperature dependence of emission spectrum for the partially coherent source designed in section II-2.b from silver, silicon and glass layers. As we have seen the inverse designed structures highlighted a strong coherence in frequency and a partial control in direction for both polarization states. Here we examine in what extent the temperature field is able to affect the thermal emission of this structure. To model the temperature dependence of silver and tungsten we use a dielectric function given by the free-electron/Drude model

$$\epsilon_{Ag} = 1 - \frac{\omega_p^2}{\omega(\omega - i\omega_c)} \quad (3)$$

while the optical properties of glass and silicon are assumed to remain constant over the temperature range we investigate. Increase in temperature causes the increase of the electron collision frequency ω_c thus increasing the absorption in the metal. Plasma frequency ω_p on the other hand, is approximately modeled as a constant over the range of temperatures. Silver dielectric function is approximately modeled¹² with Eq. 3 where

$$\omega_c(T) = \left[\frac{\omega_c(T = 300K)^{1.3}}{300} \right] T^{1.3} \quad (4)$$

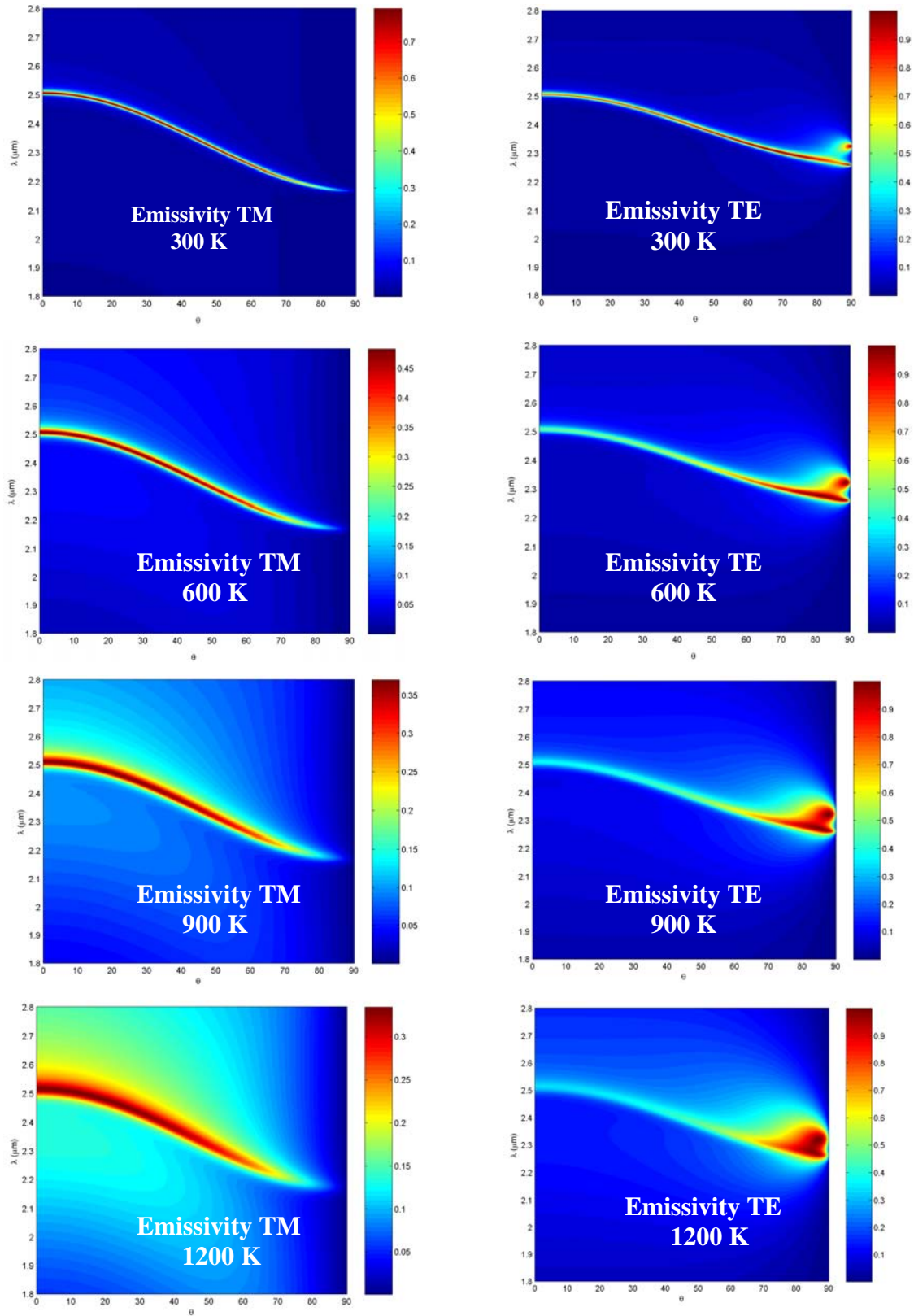


Fig.5. Thermal dependence of the emissivity spectrum in polarization TM and TE of a partially coherent thermal source made with 50 nanolayers of Ag, Si and SiO₂ layers 50 nm thick and designed by GA (cf. fig.3) .

We observe on Fig. 5 that the emissivity of the structure decreases as the temperature increases due to the increase in losses. For TM polarization the peak of emission spreads as temperature increase and the magnitude of emission strongly decreases. On the other hand, the intensity spectrum for TE polarization remains approximately constant over the operating range. However the peak of emission becomes more and more localized around the tangential direction due to the presence of plasmons modes supported by the silver layers.

These results suggest that combined with a polarizer (which can be the structure itself) it seems possible to design a polarized radiator which is able to radiate in specific direction of spaces.

III- Conclusion on the project activities, future developments and potential for ESA

Functional nanomaterials offer a unique opportunity to make breakthrough discoveries and truly revolutionary developments that are needed to succeed the energy challenge. The density functional theory developed by Kohn and Sham²¹ in the mid-60's had opened the way, by circumventing many difficulty of quantum framework, to the inverse design of nanostructured functional materials from the first principles of physics. Up to now, the ab initio design was been mainly been applied to the development of new materials with specific electronics, spintronics and magnetic properties. In the present project we have made a step towards the inverse design of functional materials for infrared (dissipative) optics. *We have reported numerical experimentations demonstrating that it is possible to predict the inner structure of nanolayered thermal sources for controlling both spatially and spectrally their emission, reflection and transmission properties simultaneously for the two states of polarization of the thermal light.*

The ability to artificially grow in a controllable manner, from modern deposition techniques (CVD, PECVD, MEB...), complex structural configurations of metallic, polar and dielectric materials raises now the issue of the 'best' achievable inner structures to tailor the radiative properties of a nanostructured thermal source in a prescribed manner and to enhance the coherence degree of its emission. Until now, this engineering design problem was unsolved. Our approach based only on the basic principles of optics is the first solution to this problem. We have demonstrated the feasibility and efficiency of ab initio design for infrared optics. However several points could be furthermore developed for a best control of emission spectra.

In particular it would be interesting to pursue the approach developed in this study to design two dimensional radiators. *Indeed, we think that an appropriate coupling of layered structures with surface gratings could improve significantly the directivity of microstructured radiators.*

From a more technical point of view, the implementation of the scattering matrix method rather the transfer matrix (see appendix) method could probably improve the stability of our design algorithm. Indeed the scattering method separate the inward from the outward waves and allow to consider very large samples without risk of diverging. Actually, due to the presence of losses, this algorithm is limited to relatively thin structures (basically between 1 to 50 μm thick).

The ab initio design technique we have developed in this project is a very powerful approach for the thermal management of satellites and generally speaking for the embarked electronic devices. Such an approach could also find broad applications in others fields of thermal sciences. For example one can consider ab initio design of functional materials to improve the performance of numerous optical technologies such as the thermophotovoltaic energy conversion, infrared spectroscopy or radiative cooling. The rational design of materials also finds numerous ramification and applications in others fields of physics. For instance, it could be used to sculpt the transport properties of nanocomposites materials by considering some of their energy carriers (electrons, photon, phonons, magnons, excitons,...) as waves moving in a scattering network. In particular, our work opens interesting prospects for thermoelectric conversion by providing a method to achieve materials with high figure of merit that is with high electric conductivity and small thermal conductivity.

APPENDIX

Calculation of thermoradiative properties

The thermoradiative properties of a multilayered medium are readily evaluated from the transfer matrix $\mathbf{T}(0,L)$ of the whole structure. True signature of corresponding optical network, this matrix relates the electric field $|E_L\rangle$ on the left-hand side of the structure to the field $|E_R\rangle$ on its right-hand side by a relation of the form $|E_L\rangle = \mathbf{T}(0,L)|E_R\rangle$. This matricial

relation is perfectly well adapted to the composition of elementary networks corresponding to a piling up process. Thus, the transfer matrix of the whole structure is the result of product $\mathbf{T}(0,L) = \prod \mathbf{T}_{\text{sub}}$ of elementary transfer matrix \mathbf{T}_{sub} which describes either the traversal of an interface between two media or the phase shift of field across a layer. It follows that the spectral and directional transmittivity $t(\lambda, \theta)$ and reflectivity $r(\lambda, \theta)$ of a structure are given in terms of transfer matrix components by $t = |1/T_{11}|^2$ and $r = |T_{21}/T_{11}|^2$. Otherwise, from Kirchoff's law, we know that the directional (polarized) and spectral emissivity $\varepsilon(\lambda, \theta)$ is given by $\varepsilon = \alpha = 1 - t - r$, where α denotes the absorptivity of the structure.

The electric field distribution within the structure when it is highlighted by an incoming field of unit magnitude is calculated using the reflectivity coefficient r of the whole structure and the partial transfer matrix $\mathfrak{T} = \mathbf{T}(0, z)$ from the highlighted side (here located at $z=0$) and the current point. It is straightforward to see that the local field is given by

$$E(z, \theta, \lambda) = \frac{\mathfrak{T}_{22} + \mathfrak{T}_{21} - r(\lambda, \theta)[\mathfrak{T}_{11} + \mathfrak{T}_{12}]}{\det \mathfrak{T}}$$

expression, as plotted in Fig.4 . We see that, in some regions, this intensity becomes significantly larger than 1 due to internal resonance phenomena. These resonances reveal the presence of couplings between localized (evanescent) modes and the incident (propagative) wave. When this mechanism takes place in a lossy material it enhances the absorption process at the frequency of localized modes and magnifies the thermal emission .

References

- ¹ R. Carminati and J.-J. Greffet, Phys. Rev. Lett. 82, 1660-1663 (1999).
- ² A. V. Shchegrov, K. Joulain, R. Carminati, and J.-J. Greffet, Phys. Rev. Lett. **85**, 1548-1551 (2000).
- ³ H. Sai, H. Yugami, Y. Akiyama, Y. Kanamori and K. Hane, J. Opt. Soc. Am. A **18**, 7, 1471-1476 (2001).

- ⁴ J. J. Greffet, R. Carminati, K. Joulain, J. P. Mulet et al., *Nature* **416**, 61 (2002).
- ⁵ K. Richter, G. Chen and C. L. Tien, *Opt. Eng.*, **32**, 1897-1903 (1993).
- ⁶ S. John, *Phys. Rev. Lett.* **58**, 2486-2489 (1987). Also, see E. Yablonovitch, *Phys. Rev. Lett.* **58**, 2059-2062 (1987). For a more recent review, see H. Benisty, S. Kawakami, D. Norris and C. Soukoulis, *Photonics and Nanostructures : fundamentals and applications* (Elsevier, 2003).
- ⁷ M. U. Pralle, N. Moelders, M. P. McNeal, I. Puscasu, A. C. Greenwald, J. T. Daly, E. A. Johnson, T. F. George, D.S. Choi, I. El-Kady and R. Biswas, *Appl. Phys. Lett.*, **81**, 25, 4685-4687 (2002).
- ⁸ L. McCall, P. M. Plazman, R. Dalichaouch, D. Smith, and S. Schultz, *Phys. Rev. Lett.* **67**, 2017–2020 (1991). E. Yablonovitch, T. J. Gmitter, R. D. Meade, K. D. B. A. M. Rappe, and J. D. Joannopoulos, *Phys. Rev. Lett.* **67**, 3380–3383 (1991).
- ⁹ P. Ben-Abdallah and B. Ni *J. Appl. Phys.* **97**, 104910 (2005).
- ¹⁰ Lee, B.J., Fu, C.J., and Zhang, Z.M. *Appl. Phys. Lett.*, **87**, 071904, (2005). See also C. J. Fu, Z. M. Zhang, D. B. Tanner *Optics Letters*, **30**, 14, 1873-1875 (2005).
- ¹¹ P. Ben-Abdallah *J. Opt. Soc. Am. A*, Vol. 21, Issue 7, pp. 1368-1371 (2004).
- ¹² I. Celanovic, D. Perreault and J. Kassakian, *Phys. Rev. B* **72**, 075127 (2005).
- ¹³ S. Enoch, G. Tayeb, P. Sabouroux, N. Guérin and P. Vincent , *Phys. Rev. Lett.* **89**, 2013902 (2002).
- ¹⁴ L. Mandel and E. Wolf, *Optical coherence and quantum optics* (Cambridge University Press, New York, 1995).
- ¹⁵ J. H. Holland, *Adaptation in Natural and Artificial Systems* (MIT Press/Bradford Books Edition, Cambridge, MA, 1992).
- ¹⁶ E. D. Palik, *Handbook of optical constants of solids* (Academic Press, London 1998).

¹⁷ S. John, Strong localization of photons in certain disordered dielectric superlattices, *Phys. Rev. Lett.* **58**, 2486-2489 (1987). Also, see E. Yablonovitch, Inhibited spontaneous emission in solid-state physics and electronics, *Phys. Rev. Lett.* **58**, 2059-2062 (1987). For a more recent review, see H. Benisty, S. Kawakami, D. Norris and C. Soukoulis, *Photonics and Nanostructures : fundamentals and applications* **2**, 57-58, (2004).

¹⁸ W. Gellermann, M. Kohmoto, B. Sutherland, and P. C. Taylor, Localization of light waves in Fibonacci dielectric multilayers, *Phys. Rev. Lett.* **72**, 633 (1994).

¹⁹ T. Hattori, N. Tsurumachi, S. Kawato, and H. Nakatsuka , Photonic dispersion relation in a one-dimensional quasicrystal, *Phys. Rev. B* **50**, 4220-4223 (1994).

²⁰ A. Della Villa et al., Band gap formation and multiple scattering in photonics quasicrystals with a Penrose-type lattice, *Phys. Rev. Lett.* **94**, 183903 (2005) and references therein.

²¹ W. Kohn and L. J. Sham, Self-consistent equations including exchange and correlation effects, *Phys. Rev. A*, **140**, 1133-1138, (1965).